Modelling shoreline changes at Northwest of Portugal using a process-based numerical model: COAST2D

Fernando Álvarez, Ph.D.[1], Shunqi Pan, Ph.D.[2], Carlos Coelho, Ph.D.[3] and Paulo Baptista, Ph.D.[4]

[1]Coastal Engineer, RPS, 140 Bundall Road, Gold Coast, Queensland, Australia, 4217.

[2]Professor, Hydro-environmental Research Centre, School of Engineering, Cardiff University, Queens Buildings, The Parade, Cardiff, CF24 3AA, UK

[3] Professor, RISCO and Civil Engineering Department, University of Aveiro, Campus Universitário de Santiago, 3810-193, Aveiro, Portugal

[4] Investigador Auxiliar, Departamento de Geociências, Centro de Estudos do Ambiente e do Mar (CESAM), Universidade de Aveiro, Campus Universitário de Santiago, 3810-193, Aveiro, Portugal

Abstract: The coastal stretch between Vagueira and Praia de Mira, northern Portugal, is subject to high-energy wave conditions. At the same time, the shoreline is a main contributor to the local economy, extensively due to tourism. Despite the shoreline is currently protected by groynes, a better understanding on the hydrodynamics and the morphodynamics in the area is crucial for coastal managers and planners. In this work it is intended to use a process-based model, COAST2D, to predict the beach morphological changes of the said sandy beach as the study site. The model is applied to simulate the morphological changes over a 4-month period between October 2013 and February 2014 to the study site, during which a series of high intensity storm events occurred along the west coasts of Europe. Model results are compared with the measurements from topo-bathymetric fieldwork campaigns. The model results show the effect of the groynes on the nearshore coastal processes under the combined wave and tide conditions. The predicted morphological changes agree well with the field measurements. The model results also show the shoreline sensibility at the study site to high-energy waves during storms, where shoreline changed it slope to adapt to the more energetic conditions. The results clearly demonstrate the capability of COAST2D in modelling the complex hydrodynamics and morphodynamics at the study site in a seasonal scale.

Keywords: sediment transport; groynes; coastal modelling; Vagueira-Praia de Mira; storm event and seasonal scale simulations

1. Introduction

Shoreline is constantly changing due to the action of wind, waves, tides and sea level variations. Coastal erosion and coastal flooding become increasingly severer and more challenging for coastal engineers and coastal zone managers to tackle. In the past decades, various coastal defence structures have been built worldwide to protect coasts and the coastal environment. These structures include sea walls, longitudinal coastal revetments and detached breakwaters, groynes or a combination of those mentioned, in addition to the soft engineering approaches, such as beach nourishment. With global warming due to the climate change, which leads to the sea level rise, the frequency and severity of the storms are expected to increase, and coasts and coastal defences become more vulnerable under the extreme storm conditions.

To ensure the coastal defence structures to be effectively functional for their design life, it requires the designers to fully understand the impacts of the defence structures on the hydrodynamics and morphodynamics in the surrounding areas, and the response of the shoreline at several time scales. In additional to laboratory experiments to detail the coastal processes for various coastal structures (Kramer et al., 2009; Faraci et al. 2014; Faraci, 2018), process-based numerical models have been widely used to describe the complex interaction between waves, tides and sediment transport, where coastal defence structures are present, and the resulting morphological and shoreline changes. This approach can be successfully applied for short-term (hours to days) and medium-term (weeks to months) forecasting, such as single or multiple storm events, often at a limited spatial scale associated with specific engineering schemes (Karunarathna et al., 2016). Examples of such models include the applications of XBeach to several sites for morphological evolutions (Roelvink et al., 2009; McCall et al., 2010; Roelvink et al, 2018), and the statistical-process based approach for beach profiles (Pender and Karunarathna, 2013). For the predictions over a longer time and space scales, hybrid modelling, also termed behaviour-oriented models have been used as are the cases of the 1- or N-line shoreline evolution models (Pelnard-Considere, 1956; Hansen and Kraus,1989; Dabees and Kamphuis, 1998; Hanson et al, 2003; Baptista et al., 2013 and Coelho et al., 2013) and the cross-shore profile evolution models of Stive and de Vriend (1995), Niedoroda et al. (2001) and Larson et al. (2016). In the latter approach, the models retain some elements of the physics in order to reduce computational costs and simplify the dynamics on the assumption that the broad scale morphological changes will be captured (Karunarathna and Reeve, 2013). More recently a new class of approach is the data-driven models in which the measurements of past conditions at a site, together with sophisticated statistical techniques, identify patterns of behaviour that are then extrapolated into the future to form a forecast (Reeve et al., 2016). Despite the potentialities of the new class of models, process based models continue to represent strong tools of prediction due to its capacity of providing valuable insights into complex processes, thus improving the level of understanding of those processes (Reeve et al., 2016). Although the processed-based models are often computationally expensive and also require extensive calibration and validation to ensure the accuracy and effectiveness, once validated, they are capable of providing the detailed interactive processes between hydrodynamics, morphodynamics and structures. The process-based models developed for the past thirty years, have mainly been focused on two-dimensional, depth averaged (2DH) schemes (Fleming and Hunt, 1976; Latteux, 1980; Coeffe and Pechon, 1982, among others). Nicholson et al. (1997) categorize the process-based models according to the manner in which the suspended component of the sediment transport is handled. Some models are based on the assumption that the suspended sediment load is a function of the local conditions only, the resulting potential (or equilibrium) transport rates being described by empirical or semi-empirical expressions (suitable for coarser sediments). Other models solve the time-dependent diffusion-advection equation for the suspended sediment concentrations to yield the dynamic sediment load (suitable for finer sediments). Process-based models have been used to simulate the features associated to offshore breakwaters in micro-tidal conditions (Nicholson et al., 1997); to forecast the behaviour of sandy beaches including outer and inner bars (van Rijn et al., 2003); to predict the complex processes associated with tidal inlets (Roelvink, 2006); to evaluate the generic effect of shore-parallel breakwaters in macro-tidal conditions (Pan et al., 2010). The application of the process-based models to simulate the behaviour of coasts with groyne fields exposed to high energetic wave regimes including extreme events have been less studied. In the present work, an existing process-based morphological model: COAST2D, which has been developed and refined in a number of research projects including the assessment of the impacts that some types of coastal structures produce on the nearshore morphodynamics is adopted. COAST2D was used to model nearshore morphodynamics behind a set of shore-parallel breakwater at Sea Palling, UK (Pan et al., 2005; Du et al., 2010) or a set of V-shaped breakwaters (Pan et al., 2013). COAST2D has been also used in assessing the behaviour of beach nourishment on a costal defence scheme under macro-tide conditions (Pan, 2011), as well as providing data to study morphological changes with statistical approach (Alvarez and Pan, 2016).

The aim of this work is to simulate the hydrodynamics and morphodynamics of a sandy beach, protected by a set of groynes, of a 9 km section exposed to the high energetic wave regimes present in the Portuguese Northwest coast (Vagueira-Praia de Mira case study) over a 4-month storm period, from October 2013 to February 2014. Field work data include the reference situations with topo-bathymetric surveys carried out at the beginning and the end of study period respectively. The model results are then compared with data obtained in the field. Specifically, the model predicts waves, currents and sediment transport rates under a period from October 2013 to February 2014, which included calm periods and storm conditions for events with approximately one-year return period and 50-year return period, to study nearshore morphological changes and the patterns of erosion and accretion in the study area at the end of the simulation period.

2. Site Description

This study focuses on a site located in the Vagueira-Praia de Mira coastal stretch, northern Portugal, as shown in Figure 1, located at some 80 km south to Leixões. Overall, this section of the coast consists of the Aveiro Harbour in the north and Praia de Mira beach in the south. In between, there are a group of 5 groynes at Costa Nova and several longitudinal revetments, and two groynes at Vagueira and Labrego together with a longitudinal revetment at Vagueira. The most recent groynes were built in 2002/2003 at Areão and Poço da Cruz (Costa and Coelho, 2013).

This site was particularly chosen because of the complex hydro-morphodynamics due to the presence of the coastal structures, as well as the availability of the field data. The Vagueira-Mira coastal stretch, located at the Northwest coast of Portugal, is a sand barrier that separates the Aveiro lagoon from the ocean. This sandy coastal system is under a very energetic wave climate, where major storms are from the Northwest quadrant, being swell-dominated with the main wave direction in WNW-NNW (Coelho and Veloso-Gomes, 2003; Coelho *et al.*, 2009). As a consequence of the wave climate, littoral drift currents also act mainly in North-South direction which has been clearly evidenced by accretion areas located at north of groins and erosion areas at the south (Dias *et al.*, 2014). Thus, this coastal stretch experiences severe erosion problems, particularly in the area between the Costa Nova and Mira beaches, which is located about 20 km south of the Aveiro harbour breakwater (Figure 1).

Figure 1 Location of the extended study area, northern Portugal.

Stated in Vitorino et al. (2002), during June and September, significant wave heights and mean periods in this region are consistently less than 3 m and 8 s, which can be regarded as relatively calm period. In other seasons, the mean significant wave heights and periods exceeds 3 m (most frequent values of 3-4 m) and 8 s (most frequent mean periods of 8-9 s). During storms, the mean significant wave heights are frequently greater than 5 m and often in exceed of 7 m. The mean wave period is approximately 13 s, with the maximum peak wave period reaching 18 s (Vitorino et al., 2002). The tides in the study site are semidiurnal, with the average spring and neap tidal ranges being 2.8 m and 1.2 m respectively.

As described in Scott et al. (2016), the winter of 2013/14, which is the period considered in this study, was a rare (approximately 50-year return period) event. The joint Hs-Tp probability of the storm named Hercules (Hs = 9 m; Tp = 23 s) on 6 January 2014 identified it as a 1:5 to 1:10 year wave event based on the data provided by the UK Met Office, in the Portuguese west coast, while the IPMA (Instituto Português do Mar e da Atmosfera) named this event as Christina (Hs = 9 m; Tp = 27 s).

Figure 2 shows that the close-up of the satellite images of the study area, including both groynes at Areão and Poço da Cruz. Two topo-bathymetric campaigns were carried out, on the 9th October 2013 and 1st February 2014, along the stretch of coast between Vagueira and Praia de Mira, as shown in Figure 2. There are two groynes in the surveyed area, which are in a slightly curved configuration against the predominant incoming wave direction, as shown in Figure 2 (inserts).

Figure 2. Satellite images for the study area and the computational domain

For the subaerial beach, the topographic surveys were performed with a prototype system (INSHORE) mounted on a four-wheel motor quad, which includes a set of Global Positioning System (GPS) antennae and a laser unit for distance measurement (Baptista et al., 2008; Baptista et al., 2011). The measurements were carried out during low-tide conditions in a dense profile grid, which included alongshore and cross-shore transects (profiles with 50 to 70 m spacing). GPS data were processed using Real-Time Kinematic RTK GPS software (Cunha, 2002) by means of an algorithm for kinematic ambiguity fixing in the two GPS L-bands frequencies L1/L2 (L1= 1572.42 MHz; L2=1227.60 MHz) (Hofmann-Wellenhof et al., 1992). The accuracy of the final Differential GPS (DGPS) positions is within 0.03 m horizontally (x and y) and 0.04 m vertically (z) (Baptista et al., 2011). Ellipsoidal heights were also converted to the national MSL altimetric datum of the Cascais tide gauge. The Triangular Irregular Networks (TIN) method (Lee and Schachter, 1980) was also used to convert data point observations to a 3D surface represented by a detailed DEM contour map (1.0 m of resolution). From the generated DEM, the shoreline position was extracted by considering the contour line of 1 m above the Mean Sea Level (Altimetric datum of Cascais tide gauge). For the submersed beach the INSHORE prototype was adapted to a vessel in which the laser unit was replaced by a single beam echo sounder. The survey domain includes the active profile above the -10 m depth. Cross-shore profiles were 500 m spaced along the study site.

Sediment size was also extensively measured in the study area (Silva et al., 2009; Narra et al., 2015), showing a high temporal and spatial variability. Within the present study area, D_{50} ranges from 0.35mm to 0.52mm. It is worth mentioning that the study site is adjacent to the Aveiro Harbour in the north, as shown in Figure 1, the breakwater in the updrift side of the harbour retains part of littoral drift, reducing the sediment supply to the down-drift coast.

3. Model Description

The COAST2D model is a 2D depth-averaged hydrodynamic and morphodynamics model, which has been well validated during its development and refinement. The model consists of a number of fully interactive modules, mainly: (1) a wave module to determine wave-period, averaged wave energy or wave height and wave direction for the wave transformation from offshore to nearshore; and a current module to compute the depth-integrated current velocity and water surface elevation under both tide and wave actions; (2) a morphological module to compute the sediment transport rates using equilibrium formulae, as well as the resulting bed level changes. The model also includes full wave-current and hydrodynamic-morphological interactions. While the further information can be found elsewhere (Pan et al., 2005, 2007; Du et al., 2010), only principal governing equations are briefly given in this paper in the following sections to the aspects of currents, waves and sediment transport.

3.1 Currents

The governing equations for the water surface elevation and 2D depth averaged currents are the continuity and momentum equations, as shown below:

$$\frac{\partial z}{\partial t}+\frac{\partial}{\partial x}(dU)+\frac{\partial}{\partial y}(dV)=0 \tag{1}$$

where: z = surface elevation; *t* = time; U, V = horizontal depth-integrated velocity components in the x and y directions; and d = water depth.

$$\begin{aligned}&\frac{\partial dU}{\partial t}+\frac{\partial dUU}{\partial x}+\frac{\partial dUV}{\partial y}-\frac{\partial}{\partial x}\left(\nu\frac{\partial dU}{\partial x}\right)-\frac{\partial}{\partial y}\left(\nu\frac{\partial dU}{\partial y}\right)+\\ &\qquad gd\frac{\partial z}{\partial x}+C_xU\sqrt{U^2+V^2}+fdV-\frac{1}{\rho}\left(\frac{\partial S_{xx}}{\partial x}+\frac{\partial S_{xy}}{\partial y}\right)+\tau_{wx}=0\end{aligned} \tag{2}$$

$$\begin{aligned}&\frac{\partial dV}{\partial t}+\frac{\partial dVU}{\partial x}+\frac{\partial dVV}{\partial y}-\frac{\partial}{\partial x}\left(\nu\frac{\partial dV}{\partial x}\right)-\frac{\partial}{\partial y}\left(\nu\frac{\partial dV}{\partial y}\right)+\\ &\qquad gd\frac{\partial z}{\partial y}+C_yV\sqrt{U^2+V^2}-fdU+\frac{1}{\rho}\left(\frac{\partial S_{xy}}{\partial x}+\frac{\partial S_{yy}}{\partial y}\right)+\tau_{wy}=0\end{aligned} \tag{3}$$

where: C_x and C_y = frictional coefficients in x and y directions for U and V respectively; ν = turbulent eddy viscosity; f = Coriolis force coefficient; S_{xx}, S_{xy}, S_{yy} = wave radiation stresses if wave computation is coupled (detailed late); τ_{wx}, τ_{wy} = wind shear stresses on the surface. If the bed form effects are not considered, the bed friction is calculated by $C_x=C_y=0.016(\Delta/d)^{1/3}$, where: Δ = roughness height, which can be related to the sediment size as $\Delta\approx 2.5D_{50}$ and D_{50} is the median grain size.

3.2 Waves

The two equations describing the wave vectors are derived from the kinematic conservation equation (Phillips, 1977):

$$\frac{\partial K_i}{\partial t} + \frac{\partial \omega}{\partial x_i} = 0 \tag{4}$$

where: K_i = wave number vector {i=1,2}; t = time; ω = apparent wave frequency; and x_i = horizontal coordinate vector. To include the effect of currents, it is assumed that the waves are propagating on a medium moving with velocity U_i. The apparent frequency is then given by the Doppler equation: $\omega = \sigma + K_j U_j$, where: σ = intrinsic wave frequency. Applying the small amplitude wave theory, the intrinsic wave frequency can be described by the linear dispersion equation: $\sigma^2 = gk \tanh(kd)$, where: k = wave separation factor.

Taking account for the wave diffraction based on the approach proposed by Battjies and Janssen (1978), for the effect of wave amplitude on the kinematics of small-amplitude waves, the wave number vectors can be calculated using:

$$K_j K_j = k^2 + \frac{1}{A}\nabla^2 A \tag{5}$$

where: A = wave amplitude. Differentiating Eq. (5) leads to the following equations for wave directions in both x and y directions respectively:

$$\frac{\partial P}{\partial t} + \left[C_g \frac{P}{k} + U\right]\frac{\partial P}{\partial x} + \left[C_g \frac{Q}{k} + V\right]\frac{\partial P}{\partial y} + \frac{\sigma G}{2d}\frac{\partial d}{\partial x} - \frac{C_g}{2k}\frac{\partial \Phi}{\partial x} + P\frac{\partial U}{\partial x} + Q\frac{\partial V}{\partial x} = 0 \tag{6}$$

$$\frac{\partial Q}{\partial t} + \left[C_g \frac{P}{k} + U\right]\frac{\partial Q}{\partial x} + \left[C_g \frac{Q}{k} + V\right]\frac{\partial Q}{\partial y} + \frac{\sigma G}{2d}\frac{\partial d}{\partial y} - \frac{C_g}{2k}\frac{\partial \Phi}{\partial y} + P\frac{\partial U}{\partial y} + Q\frac{\partial V}{\partial y} = 0 \tag{7}$$

where: P, Q = wave number vectors in x and y directions; $\Phi = \frac{1}{A}\nabla^2 A$; wave group velocity $C_g = \frac{\sigma}{2k}(1+G)$; and $G = \frac{2kd}{\sinh(2kd)}$.

For wave amplitude, the energy conservation equation for small-amplitude and linear waves in a moving medium is used as (Phillips, 1977):

$$\frac{\partial E}{\partial t}+\frac{\partial}{\partial x_i}\left(EU_i+F_i\right)+S_{ij}\frac{\partial U_j}{\partial x_i}+\tilde{D}=0 \tag{8}$$

where: E = total wave energy; F_i = wave flux vector; S_{ij} = radiation stress tensor {i=1,2}; and $\tilde{D}$ = energy dissipation due to the wave breaking and the bottom friction. Considering the relation between wave amplitude and wave energy gives the following equation:

$$\begin{aligned}\frac{\partial A}{\partial t}+\frac{1}{2A}\left\{\frac{\partial}{\partial x}\left[A^2\left(\frac{C_g}{k}P+U\right)\right]+\frac{\partial}{\partial y}\left[A^2\left(\frac{C_g}{k}Q+V\right)+\right]\right\}\\ +\frac{1}{\rho gA}\left[S_{xx}\frac{\partial U}{\partial x}+S_{xy}\left(\frac{\partial U}{\partial y}+\frac{\partial V}{\partial x}\right)+S_{yy}\frac{\partial V}{\partial y}\right]+C_aA=0\end{aligned} \tag{9}$$

where: C_a = dissipation coefficient due to the wave breaking and the bottom friction; and S_{xx}, S_{xy}, S_{yy} = wave radiation stresses given by:

$$S_{ij}=\frac{1}{2}\left[\left(1+G\right)\frac{K_iK_j}{k^2}+G\delta_{ij}\right]E \tag{10}$$

For random waves, the energy dispassion due wave breaking is considered with the approach proposed by Battjes and Janssen (1978), which can be calculated using: $\tilde{D}=\frac{\alpha\pi}{2T}Q_bH_m^2$, where: H_m = the maximum possible wave height; Q_b = the probability of wave breaking; and α = constant.

3.3 Sediment transport

The total sediment transport which includes both bed load and suspended sediment transport for combined waves and current conditions, as suggested by Soulsby (1998), is used in the model:

$$q_t=A_sU\left[\left(U^2+\frac{0.018}{C_D}U_{rms}^2\right)^{1/2}-U_{cr}\right]^{2.4}(1-1.6\tan\beta) \tag{11}$$

where:

$$A_{sb}=\frac{0.005h\left(d_{50}/h\right)^{1.2}}{\left[(s-1)gd_{50}\right]^{1.2}} \tag{12}$$

$$A_{ss}=\frac{0.012d_{50}D_*^{-0.6}}{\left[(s-1)gd_{50}\right]^{1.2}} \tag{13}$$

$$A_s = A_{sb} + A_{ss} \tag{14}$$

$$C_D = \left[\frac{0.40}{\ln(h/z_0) - 1} \right]^2 \tag{15}$$

and, q_t = the volumetric transport rate; D_* = dimensionless grain diameter; C_D = drag coefficient due to current alone; β = slope of bed in stream wise direction, positive if flow runs uphill; $\overline{U}$ = depth-averaged current velocity; U_{rms} = root-mean-square wave orbital velocity; and z_0 = roughness height. For rippled bed, z_0 is set to 6 mm.

All governing equations described above are discretised and solved using explicit finite difference methods with appropriate boundary conditions specified. All modules are fully and dynamically interacted between both hydrodynamics and morphodynamics.

4. Model Setup

In this study, the main focused modelling area is the central part of the coast between Vagueira and Praia de Mira. To drive the model, offshore wave data measured from a wave station at Leixões, located some 80km at north of Aveiro, is available for this study. Figure 3 shows the measured wave height time series at Leixões, wave directions and the correlation of wave height and wave period. Incident waves are predominately from North-west direction and the wave periods range from 5 to 15 seconds with a clear correlation with the significant wave height. The circles in Figure 3 (a and b) indicate the dates of the topo-bathymetric surveys.

Figure 3. Offshore wave conditions: (a) significant wave height (Hs); (b) wave direction; and (c) correlation between significant wave height and wave period at Leixões station (October 2013 to February 2014).

As the focus of this study is to investigate the beach morphological changes with the presence of groynes at Areão and Poço da Cruz using the fine resolution COAST2D model, it becomes necessary to carry out the modelling in two stages. The first stage is to set up COAST2D over a larger computational domain, extending from the wave buoy station at Leixões to the nearshore area with a coarser grid for simulating hydrodynamics only. The main purpose of this exercise is to transform that wave conditions measured at the wave buoy station to the open boundary of the smaller, but fine resolution COAST2D setup, for the coastal morphological simulations. The computational domain for a coarser grid is shown in Figure 4, which covers an area of 120 km in the alongshore direction and 40 km in the across-shore direction, with the respective 1 km and 0.4 km grid sizes. The COAST2D model is run over a period of 2760 hours, generating the wave conditions at location A, for the fine grid model at the second stage.

Figure 4. The computational domains of the COAST2D setups for the two stage simulations (finer-resolution domain is indicated as A).

The computed wave heights generated by COAST2D at location A for a time period between 9th October 2013 (t=0h) to 1st February 2014 (t=2760h) are compared with the measured ones at Leixões wave buoy in Figure 5, during which, three storm events occurred as indicated by the grey bands (see also Table 1).

Figure 5. The wave heights generated by COAST2D at Location A, in comparison with the measured ones. Storm events are indicated by the grey bands.

At stage two, the fine resolution COAST2D model was then set to cover the computational area of 9 km in the alongshore direction and 2.565 km in the cross-shore direction, as shown in Figure 6, with the inclusion of groynes at Areão and Poço da Cruz. The computational grid consists of 361 by 172 node points with grid sizes of 25m in the longshore direction and 15m in the cross-shore direction. A finer grid size is used in the cross-shore direction to increase the resolution to better capture the hydrodynamic and morphodynamic variations and to better present the curvature of the groynes. Bathymetry data surveyed on 9th October 2013 is interpolated as the initial bathymetry for the model, as shown in Figure 6. The water depth along the offshore (open) boundary is approximately 16 m. The model is forced by the wave and tide conditions based on the field measurements which are described in detail in the following sections.

Figure 6. Finer-resolution COAST2D computational domain and the locations of Box A (covering Poço da Cruz Groyne); Box B (covering Areão Groyne) and Box C (covering the nearshore area as shown).

Along the offshore boundary, time varying wave conditions (wave height, period and direction) are specified in 0.5 hourly intervals, based on the measurements obtained at the Leixões station, following the first stage simulations, as described previously. In this study, an M2 semidiurnal tide with a 2 m tidal range is used along the offshore boundary of the computational domain, as the representative tides at the study site. Despite the high temporal and spatial variability of the sediment size presented by Silva et al. (2009), sediment with an average D_{50} of 0.45 mm is used for the entire domain. Groynes are treated as bathymetry with increased roughness, but non-erodible, although sediment deposition on groynes is allowed. The crest level of the groynes is set to 4 m and their curvature is approximated well within the computational grid.

To facilitate the analysis of the impact the groynes have on the nearshore morphodynamics, three boxes were defined within the computational domain, as illustrated in Figure 6. Boxes A and B are centred at both groynes, expanding 500 m each way alongshore and 600m across-shore, from the berm to offshore. Box A is centred at Poço da Cruz Groyne and Box B is centred at Areão Groyne, while Box C covers the central part of the nearshore beach.

5. Results and discussion

Using the wave and tide conditions described in the previous sections, the COAST2D model is applied to the study site to stimulate the beach morphological changes over a period of about 4 months (2760 hours), corresponding to the period from the 9th October 2013 to 1st February 2014. The morphological changes along the simulated time, as well as the predicted waves and sediment transport from the model are examined in the predefined boxes A (Poço da Cruz Groyne) and B (Areão Groyne) as shown in Figure 6.

Additionally, three storm events have been defined within the 2760-hour period simulated (Table 1). Results are analysed for each of the storms to facilitate understanding how the shoreline reacts to each of the storm events. For the study area, the mean significant wave height is around 2 m (Narra et al., 2015), although during storms, wave height can reach 8 m (Costa et al., 2001). Commonly, storms last for less than 2 days. However, storms that persist for up to 5 days were already registered (Costa et al., 2001). For a storm defined as a wave field with significant wave heights greater than 3 m, the average storm duration is 60 hours (Sancho et al., 2016).

Table 1. Storm events definition, in accordance with the simulation period (see also Figure 5).

Figure 7 shows the volumetric changes of evolution for each box around the groynes during the study period. It should be noted that the volumetric changes for Box C have been scaled by 10 for the sake of clarity. Overall, results show that volume increases over the observed period, which represent general accretion. During storm 1 (250h < t < 810h), two different behaviours can be identified. Before t=500h, the maximum wave height reached a value of nearly 6 m (mean significant wave height of 3.6 m for the period 250 h < t < 500h), enter in the domain and accretion occur at similar rates in both boxes. After t=500h wave height decrease (mean significant wave height of 1.8 m for the period 500h < t < 810h). At this time, volumetric changes increase significantly in Box B (for Areão Groyne) remaining nearly constant for Box A (for Poço da Cruz Groyne). This may suggest that most of the sediments transported by longshore drift currents was trapped in the up-drift groyne (Box B) which in turns facilitates some down-drift erosion, as seen after t=500h in box A (Poço da Cruz), preventing sediment to reach Box A. It must be highlighted that the main wave direction during this first storm was from WNW (wave direction of 308º for the period 250h< t < 500h and wave direction of 310º for the period 500h < t < 810h). During the following 690h (810h to 1500h) waves gradually reduce their height and volumetric changes remain nearly constant. When the second storm reaches the domain, around t=1500h, both boxes react very similarly in terms of volumetric changes during the time period between 1500h < t < 1900h, highlighting however the fact that the box A present a consistent lower volume. Once again the wave direction during the second storm was from WNW. At t=1900h it can be seen how Box B, located updrift, reduce its volume (slight erosion). The period of time between 1900h and 1948h correspond to the storm 2 peak (significant wave height of 6.2 m and mean wave direction of 320º - NW). The change of the wave direction to a northernmost position may be the main factor to induce sediment transport previous trapped in box B to box A, since longshore drift currents should be enhanced. This sediment is placed in Box A hours later, as it can be seen a sudden small peak in the volumetric changes for Box A, right after t=2000h. Around t=2250h, the system reacts in an opposite way. Box B, located updrift, seems to be trapping the sediment therefore increasing its volume, while box A reduces slightly, as sediment is trapped upstream. A decrease of wave height (2.5 m) and wave direction (299º) may be the main factors to induce this behaviour. The last storm affects both boxes similarly. As shown by the volumetric changes in Box C, the combined effect reaffirms the results for the individual box.

Figure 7. Time series of volumetric changes within Box A (red), Box B (green) and Box C (blue).

Figure 8 shows the daily average volumetric changes at each box for each of the storms. These results should be analysed in terms of the severity of storm events and the associate mean wave direction. During the study period storm events from WNW direction (Storms 1 and 3) induce up-drift sediment retention (Box B – Areão Groyne) that promotes lower sedimentary retention in Box A. As higher is the value of significant wave height the higher is the volume trapped in the boxes. The storm event from NW direction (Storm 2) induces an up-drift sedimentary transport (Box B) which is down-drift trapped (Box A). This is due to the erosion suffered by Box B before t=2000h, moving sediments from Box B to Box A. Nevertheless. overall, Box B suffers more changes than A, which shows how the down-drift groyne area (Box A for Poço da Cruz) benefit from the protection provided by the northern groyne (Box B for Areão) which regulates the deposition and accretion downstream. Overall volumetric changes in the nearshore area, as shown in Box C, indicates a progressive accretion from three storm events.

Figure 8. Daily average volumetric changes in each box for 3 storm events.

The volumetric changes in the nearshore area (in Box C) during the simulation period, as shown in Figure 8, indicate the overall accretive nature of this coastal stretch of the coast for the storm events.

Figure 9 shows the spatial distribution of the measured and modelled morphological changes during the 2760h-period studied for a nearshore area extracted from the computational domain indicated in Figure 6. It can be seen that the model represents well the changes occurred within the domain. The erosion and accretion areas are well represented. It can be seen how major erosion affects the shoreline area updrift each groyne while erosion is limited or even turned into accretion downdrift the groynes. In general, deposition occur all over the more offshore area, which indicates the shoreline is shifting to a more gentle slope becoming a dissipative profile, as a reaction to the high energy wave climate.

Figure 9. Comparison of measured and computed morphological changes (white lines indicating the locations of groynes, and colour indicates state of morphological changes: erosion (-1), accretion (1) and no changes (0)).

Figure 10 shows the wave height distribution and modelled bathymetry for each of the boxes A and B, and for the first and last of the storms defined previously. Storm 1 has been characterized for t=456h (27 October 2014) and storm 3 for t=2430h (22 January 2015), both corresponding to the highest wave height registered for each of the storms. It must be highlight that t=456h is integrated in the period of first storm (250h < t < 500h) in which the mean significant wave height is of 3.6 m and the main wave direction is from WNW (accretion occur at similar rates in both boxes according to Figure 7); and t= 2430h is integrated in the third storm in which the mean significant wave height is of 3.9 m and the main wave direction is from WNW (accretion also occur at similar rates in both boxes according to Figure 7).

The wave height for Box A (Poço da Cruz) is shown in Figures 10a (Storm 1) and 10b (Storm 3). In both cases it can be seen how waves are being refracted by the groyne effects on the bathymetry, while quickly reducing their height. It also can be seen how the wave height isolines are nearly parallel to the initial coast (Storm 1), as a result of a smoother bathymetry, but after four months of very energetic wave conditions the bathymetry is rougher. In fact, the regular bathymetry shown in Figure 10a is not verified any more in Figure 10b. This behaviour is also seen for Box B in Figures 10c and 10d. It also can be seen in Figure 10b how the shoreline is levelled at either side of the groyne, meaning there is not significantly more erosion or accretion on each side.

Figure 10. Computed wave heights near Poço da Cruz Groyne (Box A) and Areão Groyne (Box B) during Storm 1 (t=456h; Hs=2.3 m; Tp = 14 s; Dir = 322º) and Storm 3 (t=2430h; Hs =4.4m; Tp = 15 s; Dir = 314º).

The wave height for Box B (Areão) is shown in Figures 10c (Storm 1) and 10d (Storm 3). It is remarkable how in Figure 10d the shoreline is not levelled at either side of the groyne and significant more deposition can be seen updrift of the groyne. This is due to the Areão groyne, updrift retaining a big amount of sediment to travel south towards Box A (Poço da Cruz), explaining the reduced volumetric changes in that area. The wave direction from NW (314º) can also help to justify this behaviour.

Figure 11 shows the sediment transport rates for each box during Storms 1 and 3 at the same time instants as used previously (t=456h and t=2430h).

Figure 11. Computed sediment transport rates near Poço da Cruz Groyne (Box A) and Areão Groyne (Box B) during Storm 1 (t=456h; Hs=2.3 m; Tp = 14 s; Dir = 322º) and Storm 3 (t=2430h; Hs =4.4m; Tp = 15 s; Dir = 314º).

For Poço da Cruz groyne, located at downdrift of the study area, Figure 11a (Storm 1; Hs=2.3m) shows a very regular pattern and relatively low sediment transport rates, when compared with Storm 3 as shown in Figure 11b (Hs=4.4 m). This behavior can be easily explained by the lower wave heights and consequent lower sediment transport capacity for the Storm 1 instant represented. However, the impact of the groyne in the sediment transport characteristics is similar and near the groyne head the sediment transport rates are higher in both instants, with slightly onshore direction on the updrift side of the groyne and offshore sediment transport movements at downdrift.

At Areão Groyne, the sediments transport rates as shown in Figures 11c and 11d, present also lower values and regular patterns for Storm 1 (lower wave heights). At Storm 3, higher transport rates are observed for bigger depths due to the higher wave heights, which is in correlation with the wider sediment transport patterns of more energetic wave climates. It is also observed an extension of shore where the sediment transport rates are lower, just downdrift the groyne.

6. Conclusions

A process-based numerical model, COAST2D, has been used to model the shoreline changes over a 4-month period under the combined wave and tide conditions with the presence of two groynes along the coast in Vagueira-Praia de Mira, northwest of Portugal. During the 4-month simulation period, there were a number of storms including some highly energetic ones, which were measured predominately from the north-west direction. The model results show a general shift in the beach slope towards a gentler and reflective slope. It has been seen how the updrift groyne regulates the amount of sediment reaching the downdrift area, reducing the morphological transport in the sheltered area.

Qualitatively, the computed final morphological changes from the COAST2D model agrees well with the measured data and the accretion/erosion patterns within the domain are well predicted, which clearly indicate the ability of the COAST2D model in predicting the beach morphological changes under storm conditions. Further sensitivity analysis and comparison of shoreline change may reveal it spatial variability and accuracy of the model. Nevertheless, the results clearly highlight the dynamism in the study site, which results in high volume changes across the domain and a shift in the slope in just a 4-month storm period, and hence, the importance of accurately predicting the coastal erosion for coastal engineers and managers to better assess the effectiveness of future coastal defence schemes.

The model results can be further improved by including the dynamic temporal and spatial variability of the sediment size, which was found in the study site.

References

Alvarez, F., Pan, S. (2016). Predicting coastal morphological changes with empirical orthogonal function method. Water Science and Engineering, 9(1), 14-20.

Baptista, P., Bastos, L., Bernardes, C., Cunha, T., Dias, J. (2008). Monitoring sandy shore morphologies by DGPS: a practical tool to generate digital elevation models. Journal of Coastal Research 24(6), 1516-1528.

Baptista, P., Bernardes, C., Cunha, T. R. (2011). The validation analysis of the INSHORE system - a precise and efficient coastal survey system. Environmental Monitoring and Assessment. 179(1-4), 589-604.

Baptista, P., Coelho, C., Pereira, C., Bernardes, C., Veloso-Gomes, F. (2013), Beach morphology and shoreline evolution: Monitoring and modelling médium-term responses (Portuguese NW coast study site). Coastal Engineering, 84 (2014) 23-37

Batijes, J.A., Janssen, J.P.F.M. (1978). Energy loss and ser - up due to breaking of random waves. in: Proc. Sixteenth Coastal Engrg. Conf, pp. 569-587

Coeffe, Y., Pechon, P. (1982). Modelling of sea-bed evolution under waves action. Proc. 18th Int. Coastal Eng. Conf., Cape Town, pp. 1149-1160.

Coelho, C., Lima, M., Veloso-Gomes, F. (2013). Relationship Between Cross-Shore Active Profile and One-Line Shoreline Evolution Models Performance. Journal of Coastal Research, SI65, 2107-2112.

Coelho, C., Lopes, D., Freitas, P. 2009; Morphodynamics Classification of Areão Beach, Portugal; Journal of Coastal Research, SI56, 34-38.

Coelho, C., Veloso Gomes, F. (2003). Wave climate and longshore sediment transport in the Northwest Portuguese coast. Proc. of the 3rd Symposium on River, Coastal and Morphodynamics, IAHR, Barcelona, Spain, pp. 1037-1048.

Costa, M., Silva, R., Vitorino, J. (2001). Contribuição para o estudo do clima de agitação marítima na costa portuguesa, in: 2as Jornadas Portuguesas de Engenharia Costeira e Portuária. Associação Internacional de Navegação, Sines, Portugal, p. 20.

Costa, S., Coelho, C. (2013). Northwest Coast of Portugal – Past Behavior and Future Coastal Defence Options, Journal of Coastal Research, SI 65, 921-926.

Cunha, T. (2002). High precision navigation integrating satellite information – GPS – and inertial system data, Ph.D. Thesis, Faculty of Engineering of the University of Porto, Portugal, 223 pp.

Dabees, M.A., Kamphuis, J.W. (1998). ONELINE, a numerical model for shoreline change. Proceedings of the 27th International Conference on Coastal Engineering, ASCE, Vicksburg. USA, pp. 2668–2681.

Dias, J.M., Lopes, C., Coelho, C., Pereira, C., Alves, F.L., Sousa, L.P., Antunes, I.C., Fernandes, M.L., Phillips, M.R. (2014). Influence of Climate Change on Ria de Aveiro Littoral: Adaptation Strategies for Flooding Events and Shoreline Retreat, Journal of Coastal Research, SI70, 320-325.

Du, Y., Pan, S., Chen, Y. (2010). Modelling the effect of wave overtopping on nearshore hydrodynamics and morphodynamics around shore-parallel breakwaters, Coastal Engineering, 57(9), 812-826.

Faraci, C. (2018). Experimental investigation of the hydro-morphodynamic performances of a geocontainer submerged reef. Journal of Waterway, Port, Coastal, and Ocean Engineering, 144(2): 04017045.

Faraci, C., Scandura, P. and Foti, E. (2014). Bottom profile evolution of a perched nourished beach. Journal of Waterway, Port, Coastal, and Ocean Engineering, 140(5): 04014021.

Fleming, C.A., Hunt, J.N. (1976). Application of a sediment transport model. Proc. 15th Int. Coastal Eng. Conf., ASCE, Honolulu, USA, pp. 1184-1202.

Hanson, H., Aarninkhof, S., Capobianco, M., Jimenez, J.A., Larson, M., Nicholls, R., Plant, N., Southgate, H.N., Steetzel, H.J., Stive, M.J.F., De Vriend, H.J. (2003). Modelling coastal evolution on early to decadal time scales. Journal of Coastal Research, 19, 790–811.

Hanson, H., Kraus, N.C. (1989). GENESIS: generalised model for simulating shoreline change. Technical Report CERC-89-19. Coastal Engineering Research Station, US Army Corps of Engineers, Vicksburg, USA (185 pp.).

Hofmann-Wellehof, B., Lichtenegger H., Collins J. (1992). Global Positioning System - Theory and Practice, Springer Verlag Wien New York, 326 pp.

Karunarathna, H., Horrillo-Caraballo, J., Kuriyama, Y., Mase, H., Ranasinghe, R., Reeve, D. (2016). Linkages between sediment composition, wave climate and beach profile variability at multiple timescales. Marine Geology, 381, 194-208

Karunarathna, H., Reeve, D.E. (2013). A hybrid approach to model shoreline change atmultiple timescales. Cont. Shelf Res. 66, 29–35.

Kramer, M., Zanuttigh, B., van der Meer, J.W., Vidal, C. and Gironella, F.X., 2005. Laboratory experiments on lowcrested breakwaters. Coastal Engineering, 52(DELOS Special Issue): 867-885.

Larson, M., Palalane, J., Fredriksson, C., Hanson, H. (2016). Simulating cross-shore material exchange at decadal scale. Theory and model component validation. Coastal Engineering, 116, 57-66.

Latteux, B. (1980). Harbour design including sedimentological problems using mainly numerical technics. In: Proc. 16th Int. Coastal Eng. Conf., ASCE, Sydney, Australia, pp. 2213-2219.

Lee, D. T., Schachter, B. J. (1980). Two algorithms for constructing a Delaunay triangulation. International Journal of Computer & Information Sciences 9(3), pp. 219-242.

McCall, R.T., Van Thiel de Vries, J.S.M., Plant, N.G., Van Dongeren, A.R., Roelvink, J.A., Thompson, D.M., Reniers, A.J.H.M. (2010). Two-dimensional time dependent hurricane overwash and erosion modeling at Santa Rosa Island. Coastal Engineering, 57(7), 668-683.

Narra, P., Coelho, C., Fonseca, J. (2015). Sediment Grain Size Variation Along a Cross-Shore Profile – Representative D_{50}. Jouranl of Coastal Conservation, 19, 307-320.

Nicholson, J., Broker, I., Roelvink, J.A., Price, D., Tanguy, J.M., Moreno, L. (1997). Intercomparison of coastal area morphodynamic models. Coastal Engineering, 31, 97-123.

Niedoroda, A.W., Reed, C.W., Stive,M., Cowell, P. (2001). Numericalsimulationsfor coastal tractmorphodynamic Coastal Dynamics 2001, ASCE, Lund, Sweden, pp. 403–412.

Pan, S. (2011). Modelling beach nourishment under macro-tide conditions. Journal of Coastal Research, SI64, 2063-2067.

Pan, S., Horrillo-Caraballo, J. M., Reeve, D., Simmonds, D. (2013). Morphological modelling of V-shaped submerged breakwaters. Coasts, Marine Structures and Breakwaters 2013: From sea to shore – meeting the challenge of the sea, (eds.) W. Allsop and K. Burgess, Thomas Telford Ltd, London, pp. 1300-1309

Pan, S., Li, M. Zhu, Y., O´Connor, B. A., Vincent, C. E., Taylor, J. A., Dolphin, T. J., Bacon, J. C. (2005). Effect of shore-parallel breakwaters on coastal morphology under storm conditions. Coastlines, Structures and Breakwaters 2005, (ed.) N. W. H. Allsop, Thomas Telford Ltd, London, pp. 64-73

Pan, S., Reeve, D.E., Davidson, M., O'Connor, B., Vincent, C., Dolphin, T., Wolf, J., Thorne, P., Bell, P., Souza, A., Chesher, T., Johnson, H., Leadbetter, A. (2010). Larger-scale morphodynamic impacts of segmented shore-parallel breakwaters on coasts and beaches: an overview of the LEACOAST2 Project. Shore & Beach, 78(4) /79 (1), 35–43.

Pan, S., Wolf, J., Chen, Y., Bell, P., Du, Y., Fernando, P., Li, M. (2007). Modelling nearshore waves with presence of shore-parallel breakwaters. Coastal Structures 2007, (eds.) L. Franco, G. R. Tomasicchio and A. Lamberti, World Scientific Publishing Co. Pte. Ltd, pp. 1125-1134

Pelnard-Considere, R. (1956). Essai de Theorie de l'Evolution des Formes de Ravage en Plages de Sables et de Galets. Societe Hydrotechnique de France, IV'eme Journee de L'Hydraulique Question III, Rapport, 1, 74–1-10 (in French).

Pender, D., Karunarathna, H. (2013). A statistical-process based approach for modelling beach profile variability. Coastal Engineering, 81, 19–29.

Phillips, O.M. (1977). The dynamics of the upper ocean, 2nd editon. Cambridge University Press, Cambridge; New York

Reeve, D., Karunarathana, H., Pan, S., Horrillo-Caraballo, J., Rózynski, G., Ranasinghe, R. (2016). Data-Driven and hybrid coastal morphological prediction methods for mesoscale forecasting. Geomorphology, 256, 49-67.

Roelvink, D., McCall, R., Seyedabolhossein, M., Neferhoff, N., Dastgheib, A. (2018). Improving predictions of swash dynamics in XBeach: The role of groupiness and incident-band run-up. Coastal Engineering, 134, 103-123.

Roelvink, D., Reniers, A., van Dongeren, A., Van Thiel de Vries, J., McCall, R., Lescinski, J. (2009). Modelling storm impacts on beaches, dunes and barrier islands. Coastal Engineering, 56, 1133 – 1152.

Roelvink, J.A. (2006). Coastal morphodynamic evolution techniques. Coastal Engineering 53, 277–287.

Sancho, F., Beirão, A., Neves, M. (2016). Intensidade energética sob temporais marítimos: casos de estudo de Espinho e do litoral da Ria Formosa, in: 4as Jornadas de Engenharia Hidrográfica. Instituto Hidrográfico, Lisbon, Portugal, pp. 215–218.

Scott, T., Masselink, G., O'Hare, T., Saulter, A., Poate, T., Russell, P., Davidson, M., Conley, D. (2016). The extreme 2013/2014 winter storms: Beach recovery along the southwest coast of England. Marine Geology 382, 224-241.

Silva, R., Baptista, P., Veloso-Gomes, F., Coelho, C., Taveira-Pint, F. (2009). Sediment grain size variation on a coastal strecth facing North Atlantic (NW Portugal). Journal of Coastal Research, SI56, 762-766.

Soulsby, R. (1998). Dynamics of Marine Sands, Thomas Telford Ltd

Stive, M.J.F., De Vriend, H.J. (1995). Modelling shoreface profile evolution. Marine Geology, 126, 235–248.

Van Rijn, L.C., Walstra, D.J.R., Grasmeijer, J., Sutherland, J., Pan, S., Sierra, J.P. (2003). The predictability of cross-shore bed evolution of sandy beaches at the time scale of storms and seasons using process based profile models. Coastal Engineering, 47, 295–327.

Vitorino, J., Oliveira, A., Jouanneau, J., Drago, T. (2002). Winter dynamics on the northern Portuguese shelf. Part 1: physical processes. Progress in Oceanography. 52, 129-153.

TABLE LIST

Table 1. Storm events definition, in accordance with the simulation period (see also Figure 5).

Storm	1	2	3
Start time (h)	250	1585	2390
Finish time(h)	810	2035	2490
Duration (h)	560	450	100
Duration (days)	23.33	18.75	4.17

Figure 1

Click here to access/download;Figure;Figure_01_Alvarez_et_al.pdf

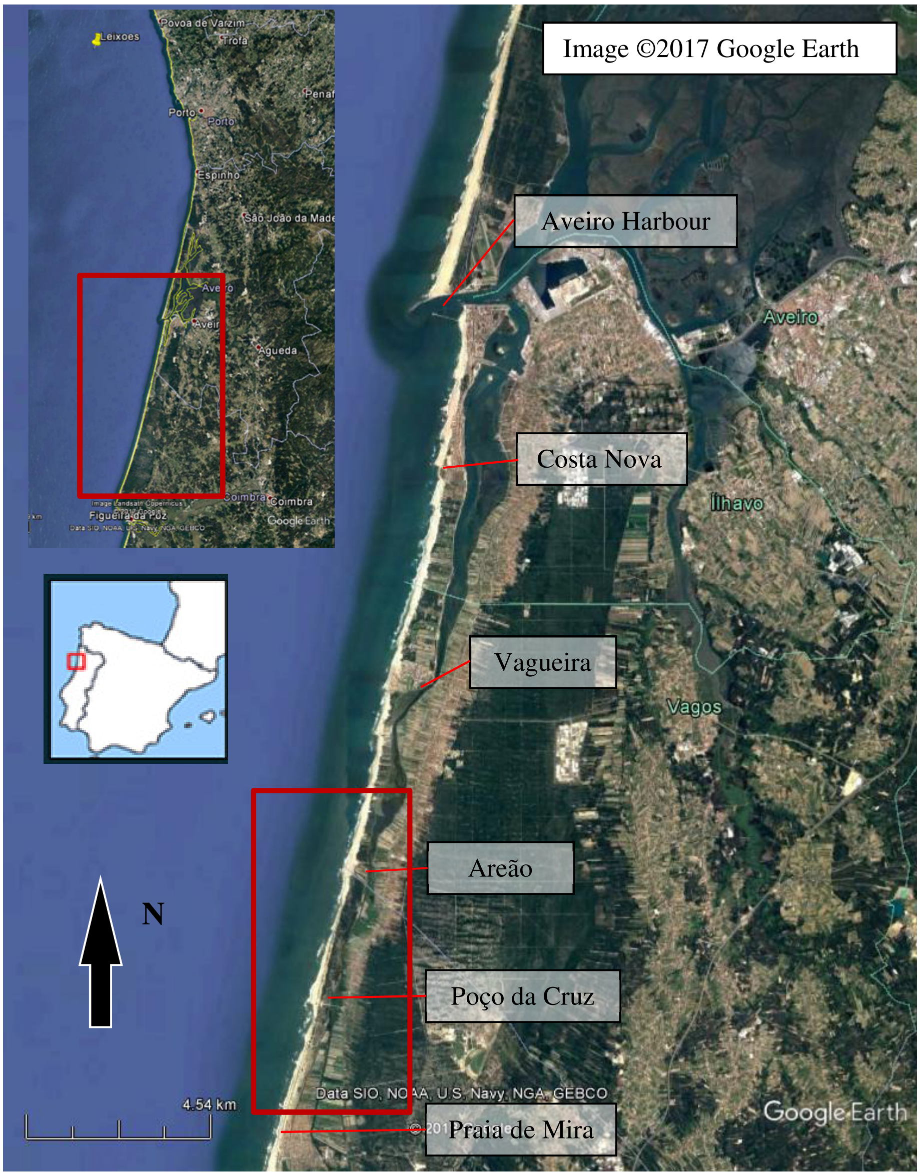

Figure 2

Click here to access/download;Figure;Figure_02_Alvarez_et_al.pdf

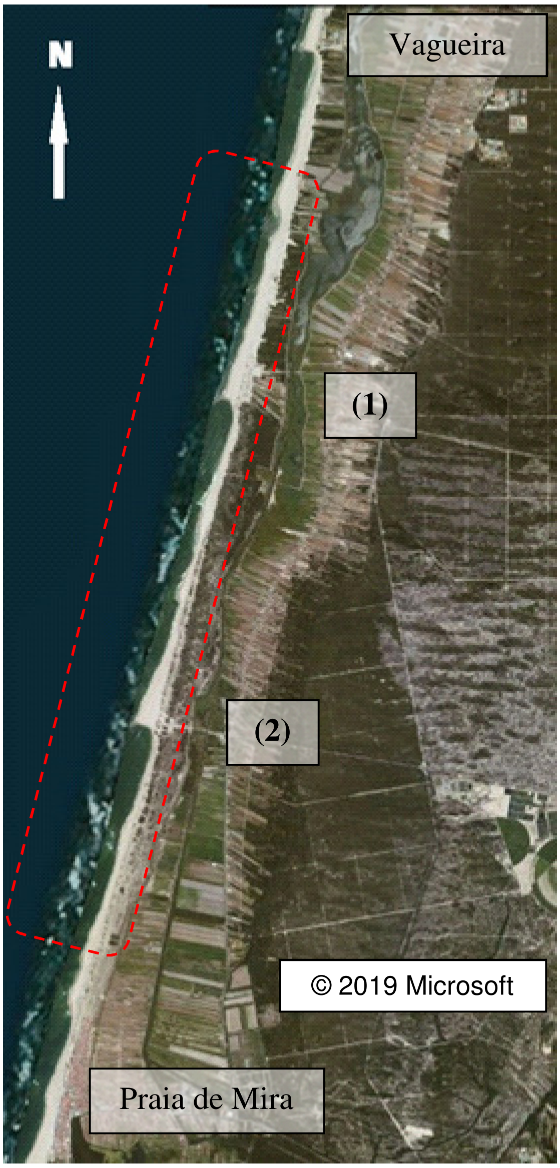

Study site and the computational domain (as boxed).

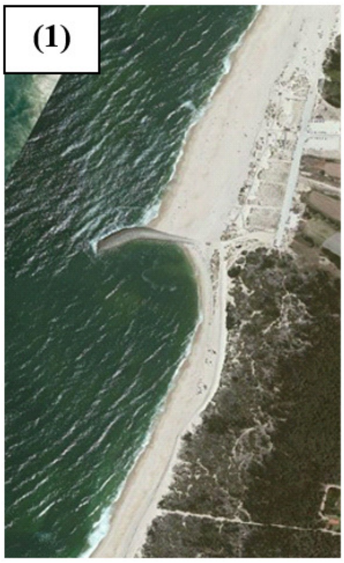

Groyne at Aerão (1)

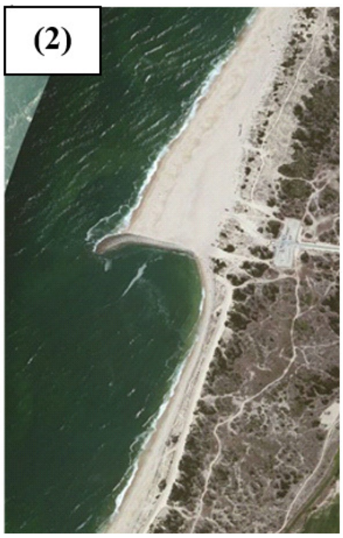

Groyne at Poço da Cruz (2)

Figure 3

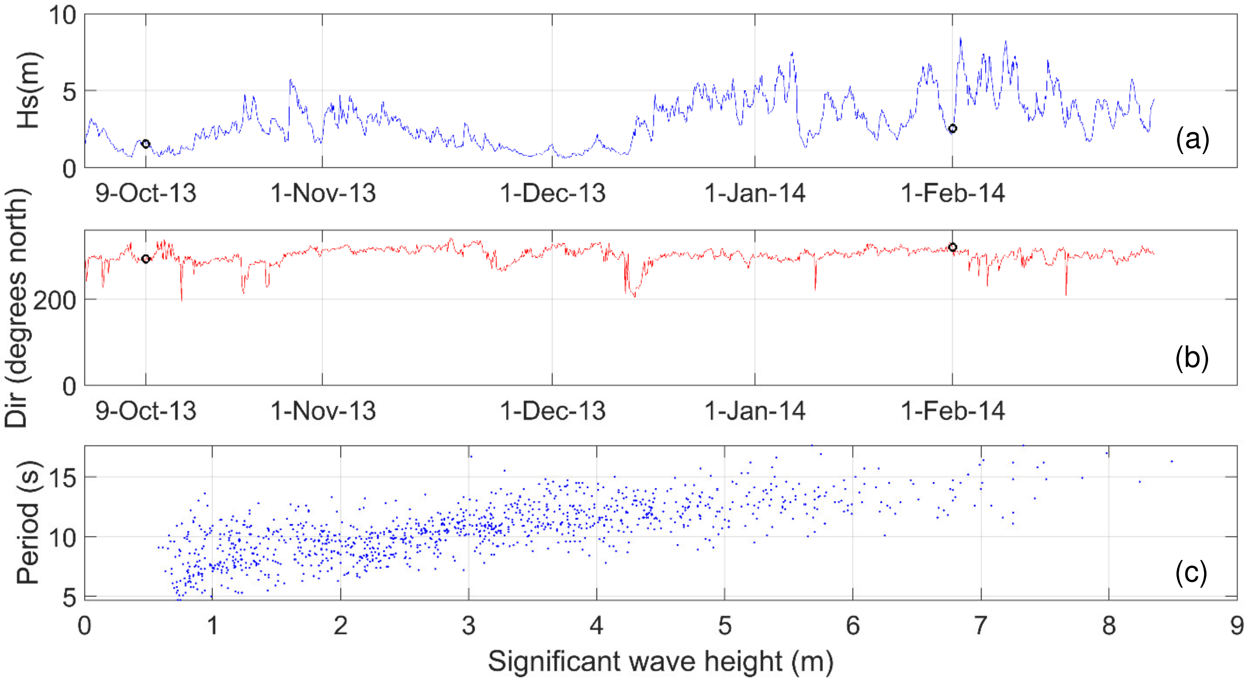
10
5
0
Hs(m)
(a)
9-Oct-13
1-Nov-13
1-Dec-13
1-Jan-14
1-Feb-14
200
0
Dir (degrees north)
(b)
9-Oct-13
1-Nov-13
1-Dec-13
1-Jan-14
1-Feb-14
15
10
5
Period (s)
(c)
0
1
2
3
4
5
6
7
8
9
Significant wave height (m)

Figure 4

[Click here to access/download;Figure;Figure_04_Alvarez_et_al.pdf]

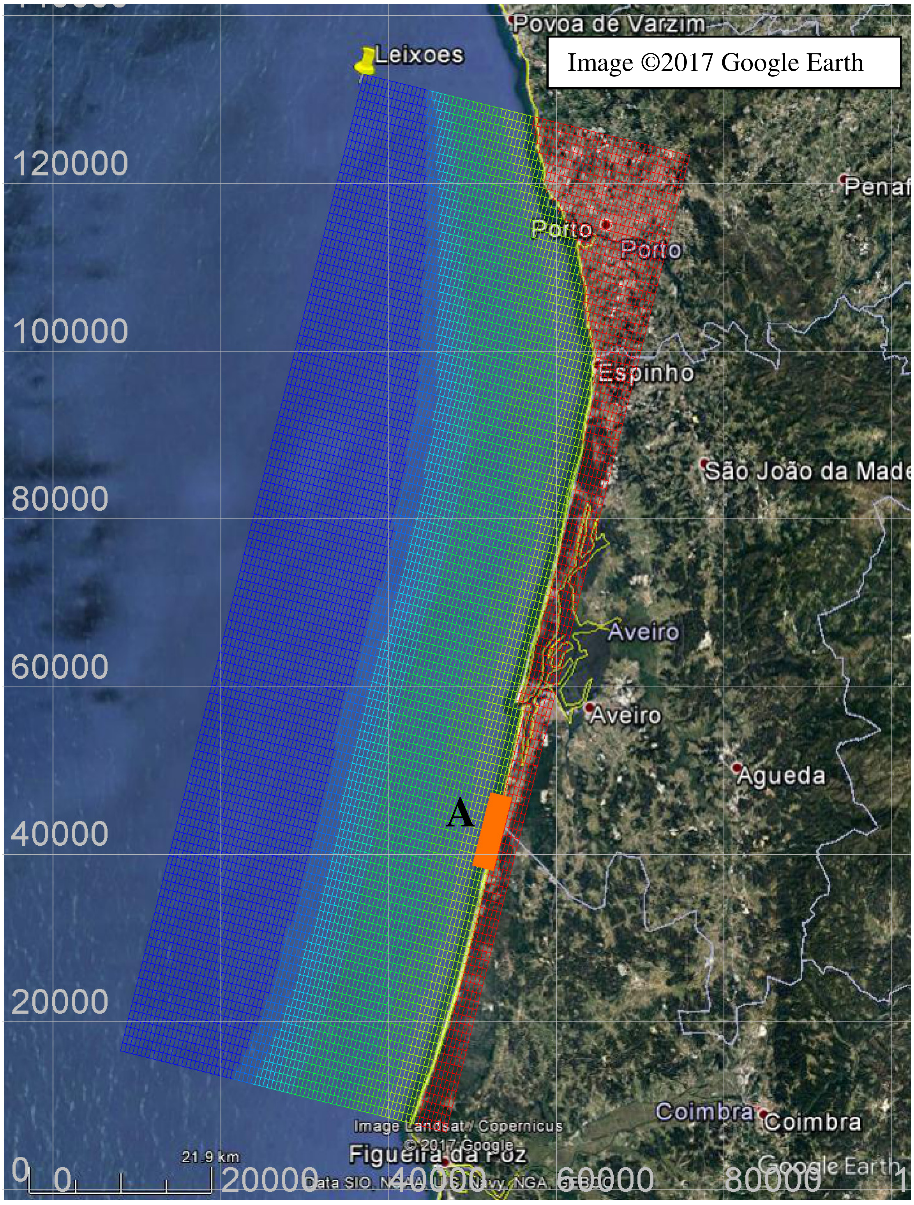

Figure 5

Click here to access/download;Figure;Figure_05_Alvarez_et_al.pdf

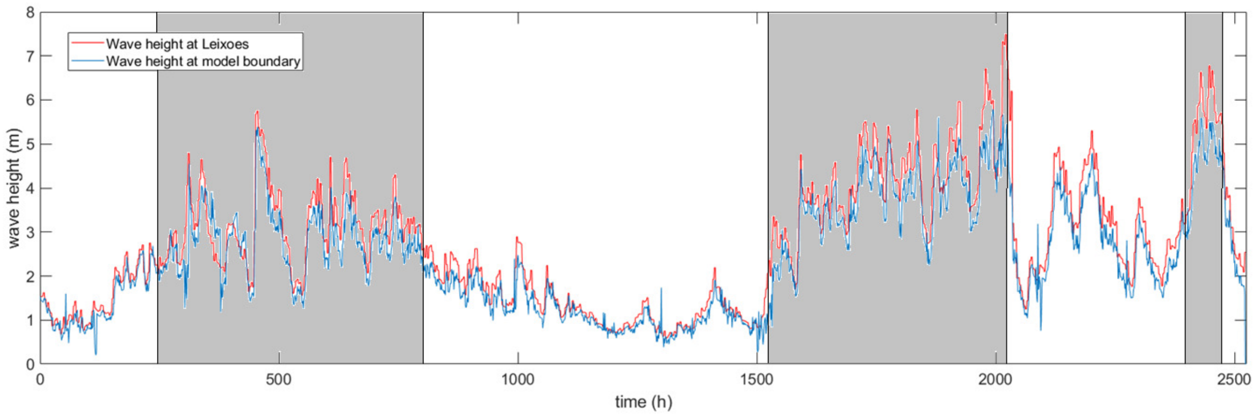

Figure 6

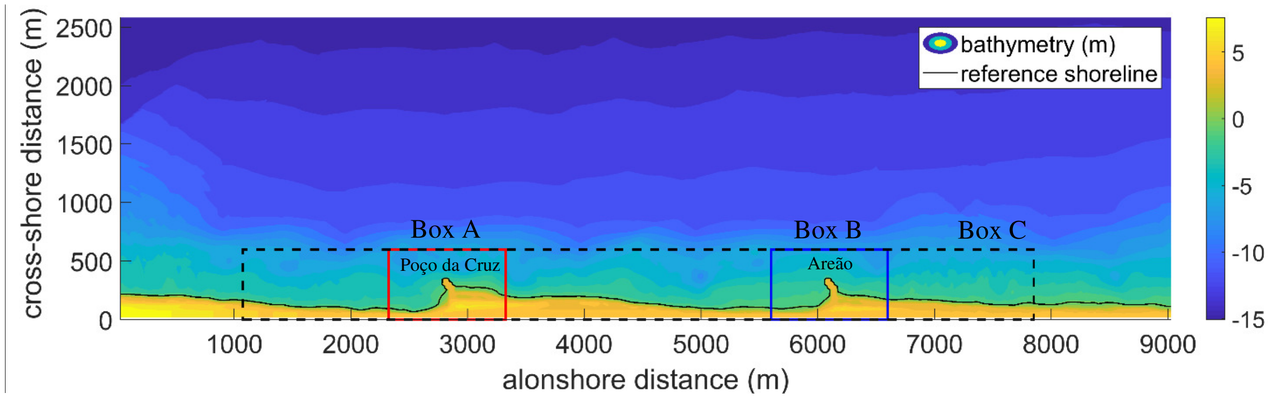
bathymetry (m)
reference shoreline
Box A
Box B
Box C
Poço da Cruz
Areão
cross-shore distance (m)
alonshore distance (m)
2500
2000
1500
1000
500
0
1000
2000
3000
4000
5000
6000
7000
8000
9000
5
0
-5
-10
-15

Figure 7

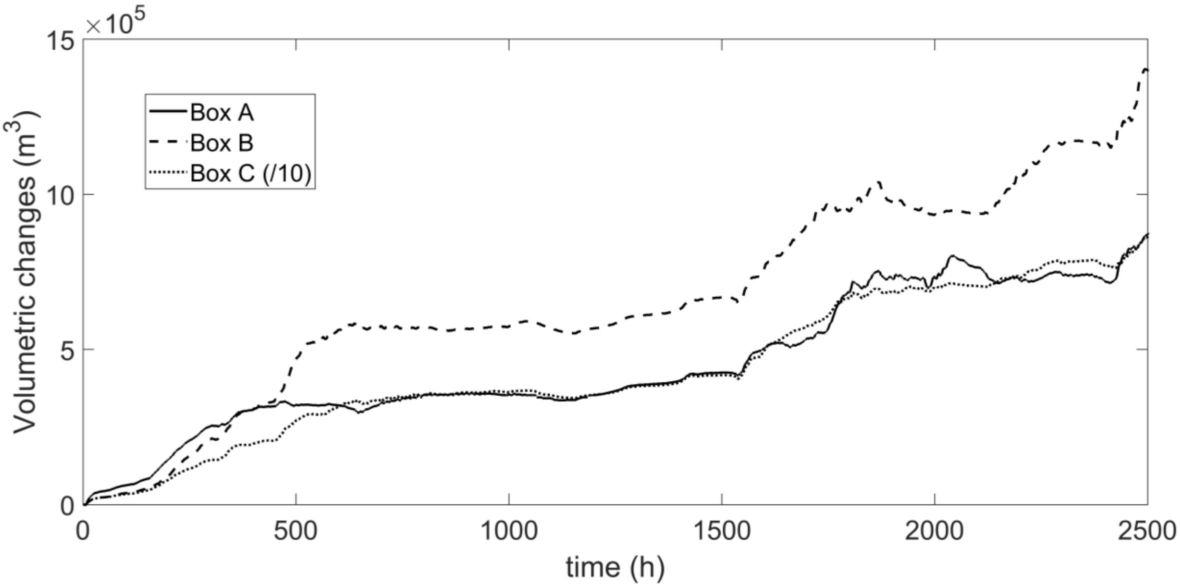

×10^5
15
10
5
0
Volumetric changes (m^3)
0
500
1000
1500
2000
2500
time (h)
Box A
Box B
Box C (/10)

Figure 8

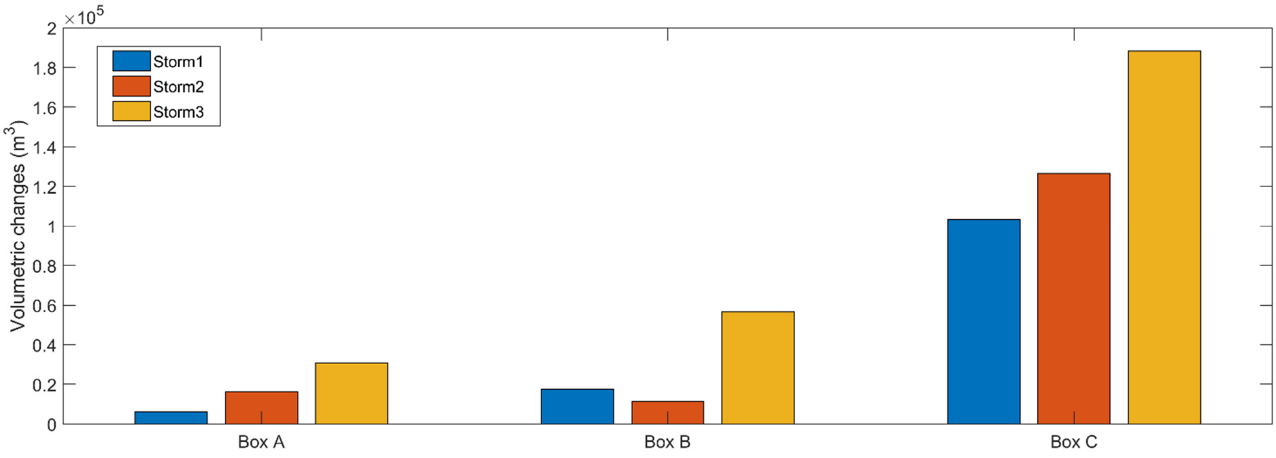
×10^5
Storm1
Storm2
Storm3
Volumetric changes (m^3)
2
1.8
1.6
1.4
1.2
1
0.8
0.6
0.4
0.2
0
Box A
Box B
Box C

Figure 9

Click here to access/download;Figure;Figure_09_Alvarez_et_al.pdf

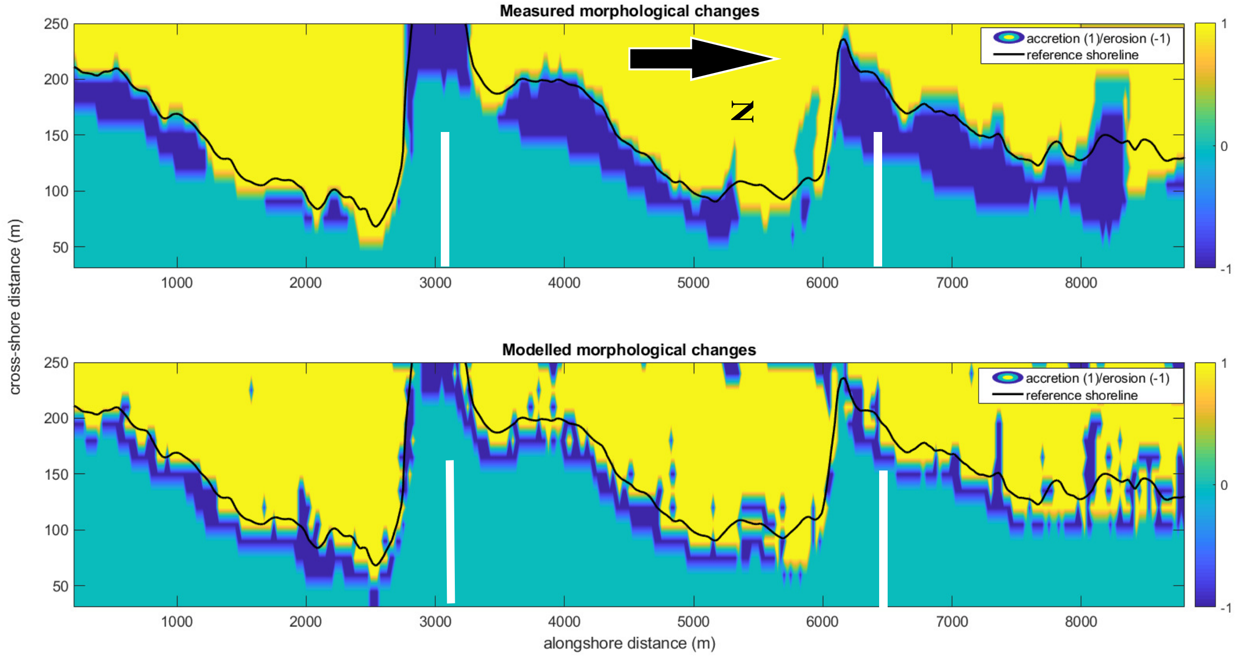

Figure 10

Click here to access/download;Figure;Figure_10_Alvarez_et_al.pdf

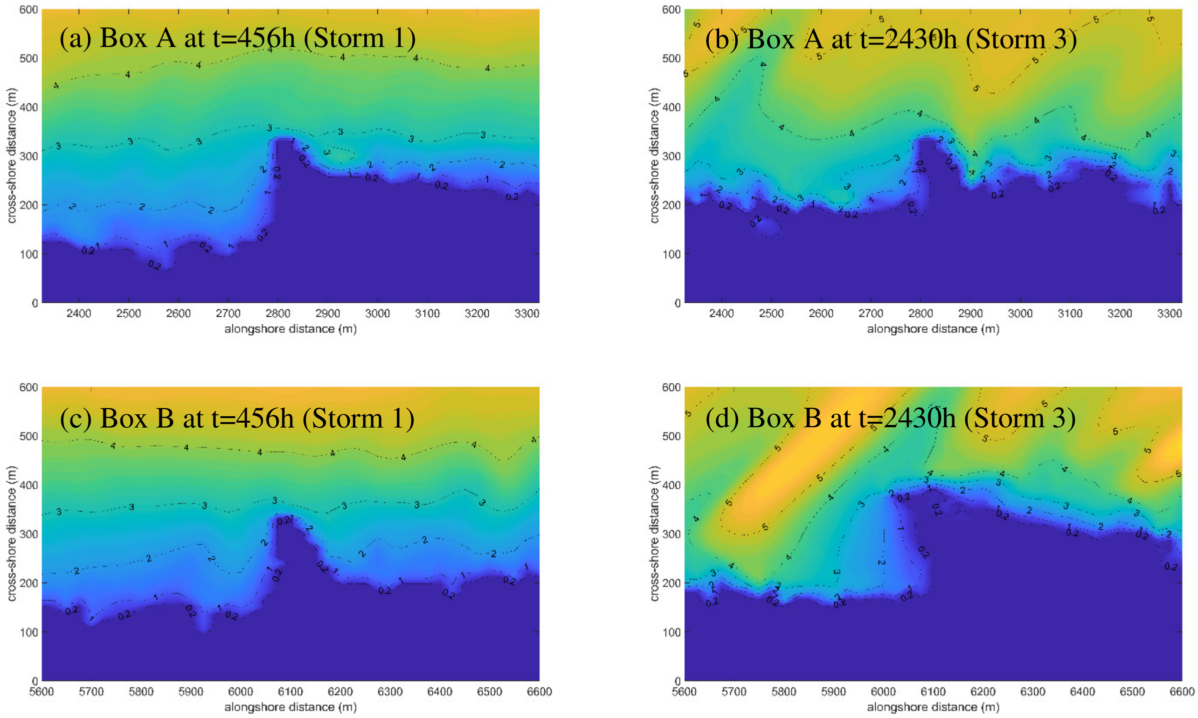

Figure 11

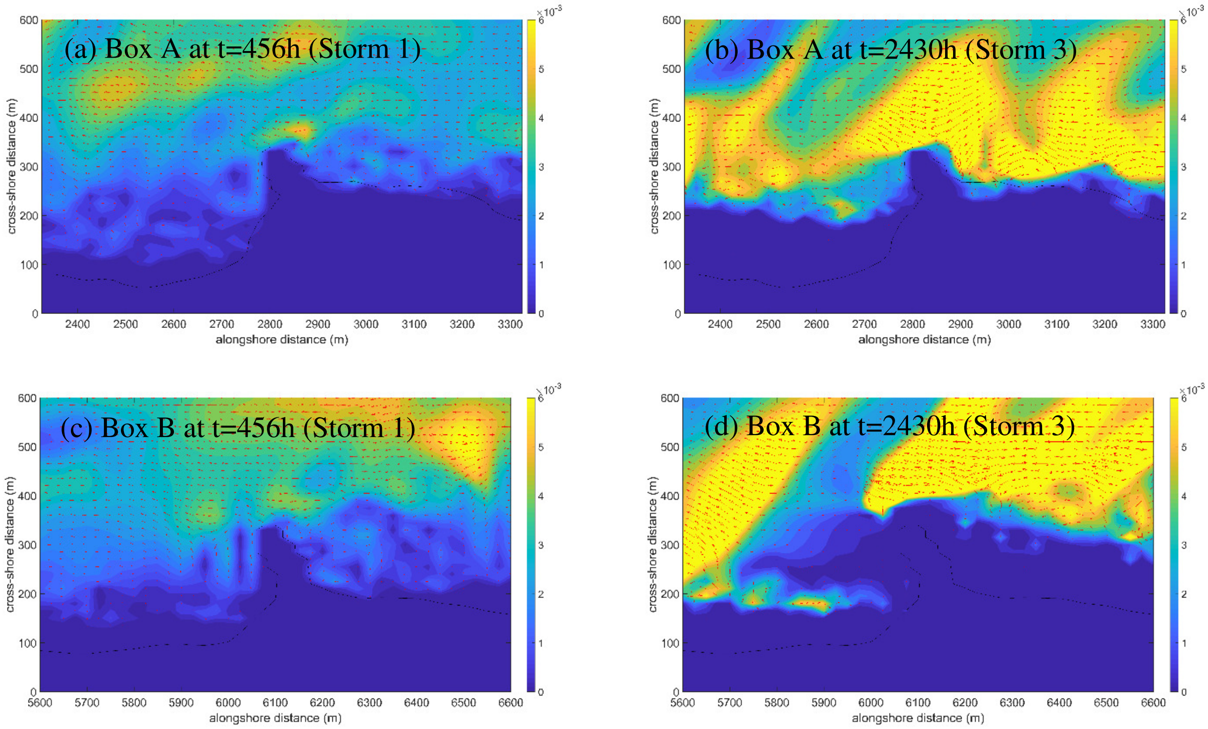
(a) Box A at t=456h (Storm 1)
(b) Box A at t=2430h (Storm 3)
(c) Box B at t=456h (Storm 1)
(d) Box B at t=2430h (Storm 3)
cross-shore distance (m)
alongshore distance (m)
$\times 10^{-3}$

FIGURE LIST